Acta Pharmaceutica Sinica B 2022;12(5):2479–2493

Chinese Pharmaceutical Association
Institute of Materia Medica, Chinese Academy of Medical Sciences

Acta Pharmaceutica Sinica B

www.elsevier.com/locate/apsb
www.sciencedirect.com

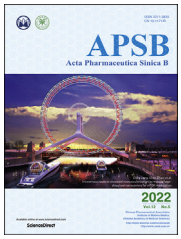

ORIGINAL ARTICLE

The long-circulating effect of pegylated nanoparticles revisited *via* simultaneous monitoring of both the drug payloads and nanocarriers

Wufa Fan[a], Haixia Peng[a], Zhou Yu[a], Luting Wang[a], Haisheng He[a], Yuhua Ma[a,d], Jianping Qi[a,c], Yi Lu[a,c], Wei Wu[a,b,c,*]

[a]*Key Laboratory of Smart Drug Delivery of MOE, School of Pharmacy, Fudan University, Shanghai 201203, China*
[b]*Center for Medical Research and Innovation, Shanghai Pudong Hospital, Fudan University Pudong Medical Center, Shanghai 201399, China*
[c]*Shanghai Skin Disease Hospital, Tongji University School of Medicine, Shanghai 200443, China*
[d]*Key Laboratory for Tibet Plateau Phytochemistry of Qinghai Province, School of Pharmacy, Qinghai Nationalities University, Xining 810007, China*

Received 25 August 2021; received in revised form 19 October 2021; accepted 25 October 2021

KEY WORDS

Long-circulating;
In vivo fate;
Aggregation-caused quenching;
Nanoparticles;
mPEG-PCL;
Doxorubicin;
Drug delivery;
Pharmacokinetics

Abstract The long-circulating effect is revisited by simultaneous monitoring of the drug payloads and nanocarriers following intravenous administration of doxorubicin (DOX)-loaded methoxy polyethylene glycol-polycaprolactone (mPEG-PCL) nanoparticles. Comparison of the kinetic profiles of both DOX and nanocarriers verifies the long-circulating effect, though of limited degree, as a result of pegylation. The nanocarrier profiles display fast clearance from the blood despite dense PEG decoration; DOX is cleared faster than the nanocarriers. The nanocarriers circulate longer than DOX in the blood, suggesting possible leakage of DOX from the nanocarriers. Hepatic accumulation is the highest among all organs and tissues investigated, which however is reversely proportionate to blood circulation time. Pegylation and reduction in particle size prove to extend circulation of drug nanocarriers in the blood with simultaneous decrease in uptake by various organs of the mononuclear phagocytic system. It is concluded that the long-circulating effect of mPEG-PCL nanoparticles is reconfirmed by monitoring of either DOX or the nanocarriers, but the faster clearance of DOX suggests possible leakage of a fraction of the payloads. The findings

*Corresponding author. Tel./fax: +86 21 51980084.
E-mail address: wuwei@shmu.edu.cn (Wei Wu).

Peer review under responsibility of Chinese Pharmaceutical Association and Institute of Materia Medica, Chinese Academy of Medical Sciences

https://doi.org/10.1016/j.apsb.2021.11.016

2211-3835 © 2022 Chinese Pharmaceutical Association and Institute of Materia Medica, Chinese Academy of Medical Sciences. Production and hosting by Elsevier B.V. This is an open access article under the CC BY-NC-ND license (http://creativecommons.org/licenses/by-nc-nd/4.0/).

of this study are of potential translational significance in design of nanocarriers towards optimization of both therapeutic and toxic effects.

© 2022 Chinese Pharmaceutical Association and Institute of Materia Medica, Chinese Academy of Medical Sciences. Production and hosting by Elsevier B.V. This is an open access article under the CC BY-NC-ND license (http://creativecommons.org/licenses/by-nc-nd/4.0/).

1. Introduction

Nowadays nano drug delivery systems are magnetizing colossal investment of resources, as witnessed by the soaring number of publications and nanomedicine products entering into different stages of the development pipeline[1−3]. Nevertheless, the total number—a few tens according to official sources worldwide—of nanomedicines that finally make to the market is exceptionally small[4−6]. The reasons behind seem to be equally intriguing to both the academia and industries. The ignorance or limited understanding of the *in vivo* behaviors of both active ingredients and nanocarriers is believed to be one of the leading reasons for the extraordinarily low translation rate[7−9].

The topic of *in vivo* behaviors or fate of drug nanocarriers is itself attractive owing to its significance in motivating not only research but also development of nanomedicines. But dismally, there are so far limited tools or strategies available to address this issue. Albeit difficult, different groups managed to carry out interesting work towards unraveling the *in vivo* fate of drug nanocarriers[10−12] by monitoring of either the drug or the nanocarriers following radioactive or fluorescent labeling[13−15]. However, the current popular strategies are concerned with crucial drawbacks. In the first place, signals of free labels could be hardly discriminated from vehicle-associated signals for both radioactive and conventional fluorescent labeling, thereby bringing about interference to bioimaging of nanocarriers[7,13,16−18]. The signals recorded are a blend of signals from both free labels and vehicles unless a workable approach is employed to discriminate the signals. Secondly, previous studies are mostly limited to qualitative analysis despite a strong demand for quantification. Failure in quantification is mainly attributed to shedding of labels, degradation of nanocarrier matrices, and the well-acknowledged concentration quenching phenomenon with regard to fluorescent labeling[7,19,20].

In recent years, the development of environment-responsive fluorescent probes opens a new era towards more accurate bioimaging of drug nanocarriers[20−24]. The signal-switching capability of fluorophores endows nanocarriers discriminability from the *in vivo* environment and, most importantly, from the signals of free, non-associated or released probes[20,23,25−28]. There are so far three types of environment-responsive fluorophores utilized for bioimaging of drug nanocarriers, that is, fluorophores with either aggregation-induced emission (AIE), Föster resonance energy transfer (FRET) or aggregation-caused quenching (ACQ) properties. For the rationale and applications of AIE- and FRET-based bioimaging, please refer to recent review articles[21,22]. Here, only the background to ACQ-based fluorescent probes utilized in this study is elaborated. ACQ is a general phenomenon associated with fluorophores which is usually regarded as unfavorable in the field of bioimaging and should be negated by all means[20,29,30]. Recently, our group synthesized a series of environment-responsive near-infrared fluorophores that have a parent structure of aza-BODIPY (4,4′-difluoro-4-bora-3a,4a-diaza-*s*-indacene). It is found that the fluorescence is able to diminish to near zero instantaneously once the fluorophores are dispersed into an aqueous media[31]. The same rationale works in a series of drug nanocarriers too[31−34]. When ACQ fluorophores are embedded in a molecularly dispersed state within the nanocarrier matrices, they emit strong fluorescence in the near-infrared range and thereby illuminate the nanocarriers[20,31,35,36]. In the meantime, non-encapsulated free fluorophores, as well as fluorophores released from nanocarriers as a result of degradation or disintegration of the nanocarrier matrices, self-assemble in the aqueous media through π–π stacking to form aggregates upon contact with water[20,37−40]. This peculiar feature of ACQ fluorophores enables more accurate bioimaging of drug nanocarriers in the biological environment with interference of non-encapsulated fluorophores reduced to a minimum[16,20,40]. By employing the ACQ-based bioimaging rationale, the *in vivo* fate of a series of drug nanocarriers has been explored[31−39,41−46].

Albeit in its infancy, investigations on the *in vivo* fate of nanomedicines are progressing steadily. So far, some facts with regard to the distribution and disposition of drug nanocarriers are clear. It is commonly acknowledged that non-decorated nanocarriers made from synthetic polymers such as polystyrenes and polyesters are readily captured by the mononuclear phagocytosis system (MPS) and cleared rapidly from the blood, whereas nanocarriers decorated with hydrophilic polymers such as polyethylene glycols (PEG) display prolonged circulation time in the blood and thereby are able to be delivered to organs and tissues beyond the MPS such as tumors[47,48]. Long circulation is an aged yet not obsolete concept. Application of new technologies of bioimaging and quantification instills refreshing understanding regarding the *in vivo* behaviors of drug nanocarriers. In early times, exploration of the long-circulating effect depends solely on monitoring of the drug payloads or emissive labels such as a fluorophore or an isotope. Nevertheless, the information thus obtained is often biased owing to drug release or label detachment. In our previous studies[48,49], the long-circulating effect of model pegylated polymeric micelles and nanoparticles was reassessed by monitoring of integral nanoparticles, but the analysis is preliminary and demands more accurate explanation based on quantitative information of both drug payloads and nanocarriers.

Herein, the current study revisits the long-circulating effect based on monitoring of both active ingredients and nanocarriers. The purpose is not only to reassess long circulation but also to explore crucial new information that deviates from conventional perception (Fig. 1). A chemotherapeutic drug, doxorubicin (DOX), that has severe organ toxicity, especially cardiotoxicity, is employed as the model drug, whereas methoxy polyethylene glycol-polycaprolactone (mPEG-PCL) polymeric nanoparticles with different degrees of PEG coating are employed as the model nanocarriers. The polymer mPEG-PCL is of good biocompatibility and biodegradability, and mPEG-PCL-based polymeric nanoparticles have been established as a reliable model with

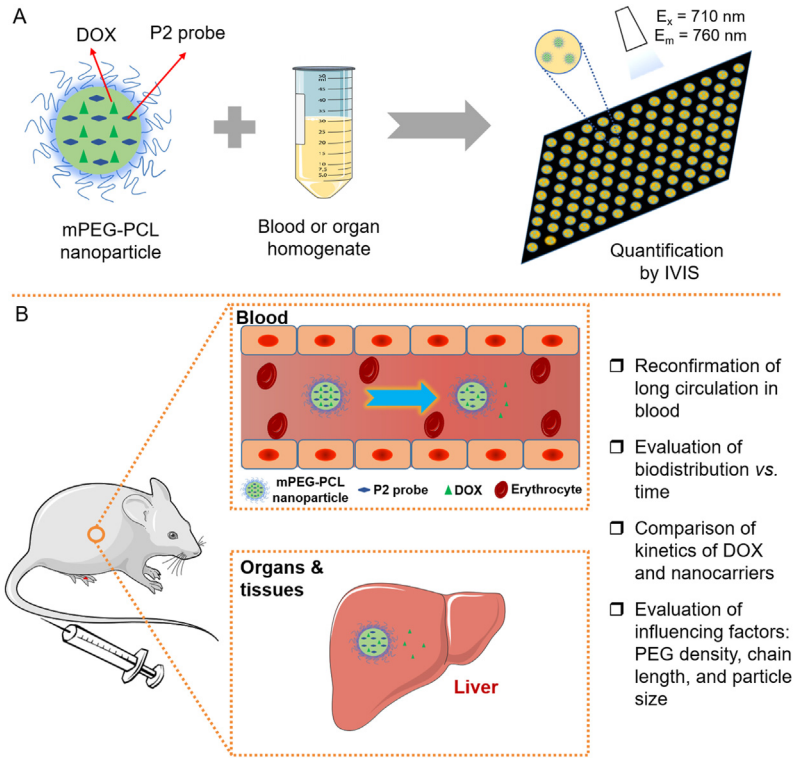

Figure 1 Schematic illustration of the rationale of quantification of mPEG-PCL nanoparticles by IVIS (A) and the objectives of this study (B).

regard to labeling by ACQ-based fluorophores[48]. Labeling the vehicles by an ACQ fluorophore, P2, enables establishment of the linearity between the fluorescence intensity and the weight of the nanoparticles and therefore quantification of the nanoparticles in the blood and various organs and tissues (Fig. 1).

2. Materials and methods

2.1. Materials

DOX hydrochloride (>99.0% purity) was purchased from Beijing HVSF United Chemical Materials Company (Beijing, China). Polyvinyl alcohol (PVA, Mn = 13,000−23,000) and poly (ε-caprolactone) (PCL, Mn = 45,000) were purchased from Sigma−Aldrich (St. Louis, MO, USA). mPEG-PCL copolymers ($mPEG_{5k}$-PCL_{45k}, $mPEG_{2k}$-PCL_{45k}) were kindly gifted from Professor Zhiyong Qian at the State Key Laboratory of Biotherapy and Cancer Center, West China Hospital, Sichuan University, Chengdu, China. The water-quenching near-infrared fluorescent probe, P2 ($\lambda_{abs}/\lambda_{em}$ = 710/760 nm), was synthesized according to previous procedures[50,51]; please refer to previous publications for its physicochemical properties[20,31]. Other chemical reagents were of at least analytical grade and purchased from Sinopharm Chemical Reagent Company (Shanghai, China). Deionized water was prepared using a Milli-Q purification system (Millipore, Billerica, MA, USA).

2.2. Animals

Studies on kinetic profiling of both DOX and mPEG-PCL nanoparticles were carried out on male SD rats weighing 200 ± 20 g (Shanghai Laboratory Animal Research Center, Shanghai, China). *In vivo* live imaging and *ex vivo* biodistribution experiments were carried out on male BALB/c mice weighing 20 ± 2 g (Shanghai Laboratory Animal Research Center, Shanghai, China). Animals were raised in the Experimental Animal Centre of Fudan University regarding the ethical guidelines on experiments involving use of animals. All experimental procedures involving use of animals were approved by the Institutional Animal Care and Use Committee at School of Pharmacy, Fudan University, China.

2.3. Preparation of DOX-loaded mPEG-PCL nanoparticles

DOX-loaded and P2-labeled mPEG-PCL nanoparticles were prepared by an emulsification/solvent evaporation method[48]. Briefly, 200 mg PCL, certain amount of mPEG-PCL, 8 mg desalted DOX base and appropriate amount of P2 (1.5‰ of total solid, *w*/*w*) were dissolved in 5 mL dichloromethane as the oil phase. PVA solution (3%, *w*/*w*) of 20 mL was utilized as the aqueous phase. Crude emulsions were prepared through homogenization by a high-shear homogenizer (Scientz Biotechnology Co., Ltd., Ningbo, China) after pouring the oil phase into the aqueous phase. Then, the crude emulsions were homogenized through a high-pressure homogenizer (AH 100 D; ATS Engineering Inc., Brampton, ON, Canada) to obtain 80 nm mPEG-PCL nanoparticles with different PEG chain lengths (5k and 2k) and different coating densities [percent of mPEG-PCL in the nanocarrier matrices (29%, 17%, 9%, and 0%, *w*/*w*)] at 1200 bar for 3 min. To prepare mPEG-PCL nanoparticles with a size of approximately 200 nm, the crude emulsions were homogenized by an ultrasonic homogenizer (Scientz IID, Scientz Biotechnology Co., Ltd., Ningbo, China) at 540 W for 3 min. An ultrafiltration device (MWCO 100 kDa, Millipore Amicon Ultra, Merck, Germany) was employed to remove non-encapsulated DOX and concentrate the nanoparticle suspension.

2.4. Characterization of mPEG-PCL nanoparticles

The average size, polydispersity index (PDI), and zeta-potential of mPEG-PCL nanoparticles were measured at 25 °C, in triplicate, using a Malvern Zetasizer Nano® (Malvern Instruments, Malvern, UK). Briefly, mPEG-PCL nanoparticle suspensions were diluted by purified water (0.1 mL dispersed in 1.9 mL water). The morphology of mPEG-PCL nanoparticles was characterized by a JEM-1230 transmission electron microscope (TEM) (JEOL, Tokyo, Japan).

The encapsulation efficiency (EE, %) and drug loading (DL, %) of DOX in mPEG-PCL nanoparticles was determined by an ultrafiltration method[52]. DOX-loaded mPEG-PCL nanoparticle suspensions were centrifugated at 3500 rpm (TGL-16G Centrifuge, Shanghai Anting Scientific Instrument Factory, China) using an ultrafiltration device (MWCO 100 kDa, Millipore Amicon Ultra, Merck, Germany) to separate free DOX from nanoparticles. DOX was analyzed by an HPLC method with Agilent 1260 series HPLC system (Agilent Technologies, Santa Clara, CA, USA) composed of a quaternary pump, a degasser, an autosampler, a column heater, a C18 column (2.1 mm × 10 mm, 3.5 μm, Agilent Eclipse, Santa Clara, CA, USA), and a tunable fluorescent detector (1260 FLD Spectra, Agilent Technologies, Santa Clara, CA, USA)[53]. The mobile phase was acetonitrile/phosphate buffered saline (PBS) (50 mmol/L $NaH_2PO_4 \cdot 2H_2O$, pH = 2.8) with a ratio of 30/70. The E_x/E_m of fluorescence detection of DOX was set to 480/560 nm, and the sample injection volume was 50 μL. EE (%) and DL (%) were calculated according to the following Eqs. (1) and (2), respectively:

$$\text{EE}\ (\%) = [(W_T - W_F)/W_T] \times 100 \quad (1)$$

$$\text{DL}\ (\%) = [(W_T - W_F)/(W_T - W_F + W_M)] \times 100 \quad (2)$$

where W_T is the total weight of DOX in mPEG-PCL nanoparticle suspension, W_F refers to the weight of non-encapsulated free DOX, and W_M is the total weight of materials including both PCL and mPEG-PCL.

2.5. In vitro drug release

DOX solution or DOX-loaded mPEG-PCL nanoparticles, equivalent to approximately 72 μg DOX, were sealed in dialysis bags (MWCO 3500), and drug release was measured in 30 mL of PBS (pH = 7.4). The release test system was shaken horizontally at 100 rpm in a water-bath oscillator thermostatically maintained at 37 °C. At pre-set time intervals, 1 mL sample was withdrawn with an equal volume of blank PBS replenished simultaneously. DOX concentration in the samples was analyzed by HPLC according to the procedures described above.

2.6. Quantification of mPEG-PCL nanoparticles in the blood and tissue homogenates

Quantification of mPEG-PCL nanoparticles in both the blood and various tissues was attained by establishing linearity between particle-bound fluorescence intensity and the concentration of nanoparticles. The concentration of mPEG-PCL nanoparticles, which is expressed as the concentration of the constituting materials, was calculated based on calibration curves.

Blood was collected into tubes pretreated with heparin from the eye sockets of male SD rats. The heart, liver, spleen, lungs and kidneys were dissected, washed, weighted and homogenized with five volumes of physiological saline after sacrificing BALB/c mice by cervical dislocation. The suspension of mPEG-PCL nanoparticles was mixed with the blood or tissue homogenates to obtain calibration samples at a series of concentrations (0.0048, 0.0098, 0.02, 0.04, 0.078, 0.156, 0.312, 0.625, 1.25, and 2.50 mg/mL). The fluorescence intensity of 100 μL samples was measured by IVIS Spectrum Live Imaging System (PerkinElmer, Waltham, MA, USA)[31,35]. The calibration curve was obtained by linear regression of fluorescence intensity *vs.* nanoparticle concentration. The quantification method was validated following protocols utilized for evaluation of conventional analytical methods.

2.7. Determination of doxorubicin in biological samples

An HPLC method was established for the determination of DOX in the blood and tissue homogenates of heart, liver, spleen, lungs, and kidneys. The biological samples were obtained according to the procedures described in Section 2.6. Briefly, 300 μL of the whole blood or tissue homogenates was extracted with 4 mL of methanol/chloroform (1/4, *v*/*v*) under vortex mixing for 3 min after addition of 100 μL daunorubicin solution (DNR, 6 μg/mL, used as the internal stand). Then, the supernatant layer of organic solvent was collected after centrifugation at 10,000 rpm (TGL-16G centrifuge, Shanghai Anting Scientific Instrument Factory, Shanghai, China) for 10 min and volatilized afterwards through nitrogen blowing. The residues were re-dissolved with 100 μL methanol. DOX in samples was determined by an HPLC method. To establish a calibration curve, 100 μL of different concentrations (10, 5, 2.5, 1.25, 0.625, 0.313, 0.156, 0.078, 0.039, and 0.0195 μg/mL) of DOX solution were added to the blood or tissue homogenates and processed as described above.

2.8. Kinetic profiling of DOX-loaded mPEG-PCL nanoparticles

For kinetic profiling, 1 mL of DOX-loaded mPEG-PCL nanoparticles, equivalent to 40 mg PCL and 350 μg DOX, of different PEGylation degrees (PCL-80 nm, $mPEG_{5K}$-9%-80 nm, $mPEG_{5K}$-17%-80 nm, $mPEG_{5K}$-29%-80 nm, $mPEG_{2K}$-29%-80 nm, $mPEG_{5K}$-29%-200 nm) were intravenously injected into rats through the tail vein with 1 mL of DOX solution, equivalent to 350 μg DOX, as a control. Blood samples (500 μL) were collected from the eye sockets at predetermined time points after injection. While 100 μL of blood samples were taken to quantify mPEG-PCL nanoparticles, 300 μL of blood samples were analyzed for DOX content.

2.9. In vivo live imaging

Before the experiment, the hair on the abdominal side of the mice was removed by depilatory cream to reduce hair-derived autofluorescence, and blank images of rats were captured before administration of nanoparticles using IVIS Spectrum Live Imaging System at the Ex/Em (710 nm/760 nm) wavelengths of P2. Then, mPEG-PCL nanoparticles, equivalent to 40 mg/mL PCL, were intravenously injected into the mice *via* the tail vein. The fluorescence images of the mice were captured at various time points after injection using IVIS Spectrum Live Imaging System. During the imaging process, animals were anesthetized by an online gas anesthesia system using isoflurane.

2.10. *Ex vivo* bioimaging and distribution of DOX mPEG-PCL nanoparticles

For the observation of biodistribution, 0.2 mL of DOX-loaded mPEG-PCL nanoparticles (40 mg/mL PCL; 350 μg/mL DOX) and DOX solution (350 μg/mL DOX) were intravenously injected into the mice through the tail vein, respectively. The mice, three per group, were sacrificed at predetermined time points after injection and the main organs and tissues (heart, liver, spleen, lungs, kidneys, brain, adrenal glands, vertebra, skin, stomach, intestine, testicles and crus) were removed, washed, weighed and placed in black plates to acquire fluorescence images using IVIS Spectrum Live Imaging System. Then, the content of mPEG-PCL nanoparticles and DOX in tissue homogenates were analyzed according to the procedures described above.

2.11. Statistical analysis

Microsoft Office Professional Plus Excel 2019, Graphpad 8 and Endnote X8 software were used for data processing and statistics, and data were shown as mean ± SD. Grouped comparisons were taken by two-tailed, unpaired Student's *t*-test. $P < 0.05$ was consider to be statistically significant.

3. Results and discussion

PCL nanoparticles with or without PEG decoration were prepared by an emulsification/solvent evaporation method[48]. To evaluate the effect of PEG decoration on the long-circulating effect of nanoparticles, block mPEG-PCL copolymers of different content (9%, 17%, and 29%, *w*/*w*) and different PEG molecular weight ($mPEG_{2k}$ *vs.* $mPEG_{5k}$) were incorporated into the PCL matrices. Moreover, the performance of nanoparticles of different sizes was compared. The physicochemical characteristics of mPEG-PCL nanoparticles are summarized in Fig. 2 and Table 1. The target size of mPEG-PCL nanoparticles is approximately 80 or 200 nm as designed with PDI values approximately 0.1 for all formulations, which indicates narrow particle distribution. The zeta-potential of mPEG-PCL nanoparticles is close to neutral, which precludes the potential influence of surface charges during comparison. The EE% of DOX in mPEG-PCL nanoparticles is approximately 20% in all 80 nm groups and 36% in the 200 nm group. The DL% of DOX in mPEG-PCL nanoparticles is less than 1.00% in all groups due to the low encapsulation efficiency of DOX. The mPEG-PCL nanoparticles exhibit strong fluorescence after labeling by P2. The fluorescence intensity has been adjusted to similar levels to avoid potential errors during comparison between groups. The TEM images show that mPEG-PCL nanoparticles have well-defined, spherical morphology with sizes similarly to those measured by a Malvern Nanosizer (Fig. 2A).

Owing to the water-quenching properties based on the ACQ effect of fluorophores[20,31], the fluorescence intensity of P2-labeled nanoparticles can be utilized to represent the quantity of nanoparticles if linearity is established[37,38,48,49]. With regard to a specific nanocarrier, the fluorescence stability is a prerequisite to establishment of a good linearity. Herein, the fluorescence stability of P2-labeled nanoparticles was verified by incubating the nanoparticles with purified water, PBS (pH = 7.4), and rat plasma at 37 °C, and the profiles of fluorescence intensity *vs.* time were monitored by an IVIS-based method[37,38]. Approximately 95% of

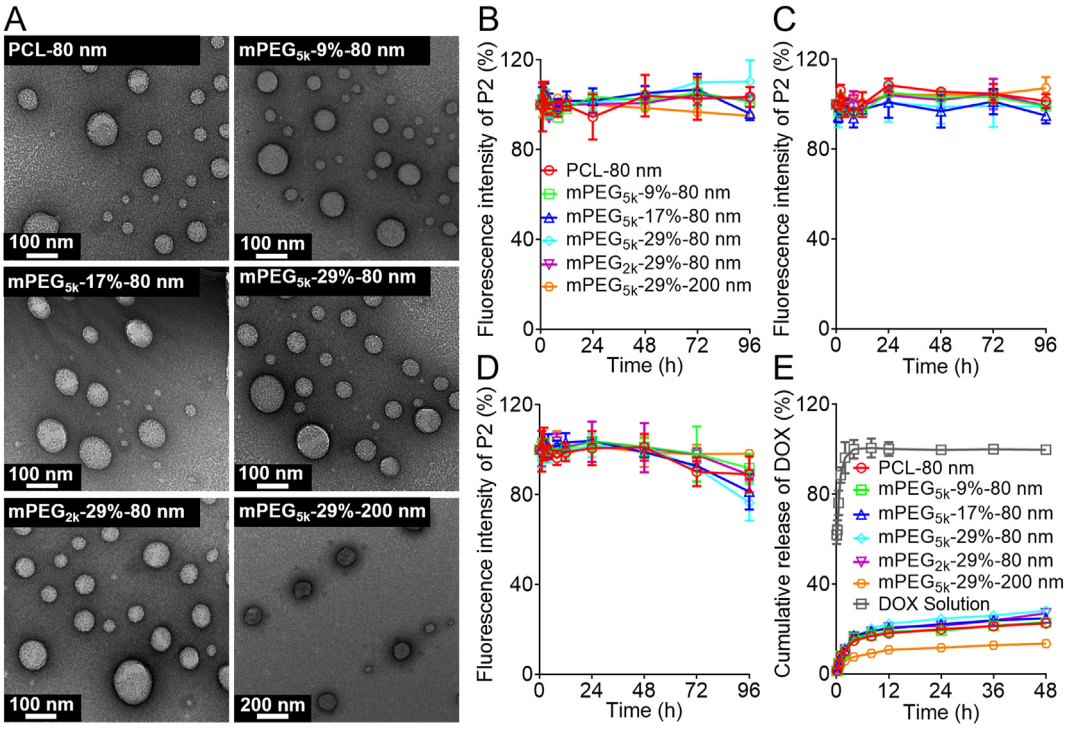

Figure 2 Characterization of P2-labeled DOX-loaded mPEG-PCL nanoparticles. (A) TEM images. (B−D) fluorescence stability in different media (B, purified water; C, PBS with pH = 7.4; D, rat plasma). (E) *In vitro* release profiles of DOX from mPEG-PCL nanoparticles in PBS (pH = 7.4). Data are presented as mean ± SD ($n = 3$).

Table 1 Characterization of DOX-loaded mPEG-PCL nanoparticles[a].

Parameter	PCL-80 nm	$mPEG_{5k}$ -9%-80 nm	$mPEG_{5k}$ -17%-80 nm	$mPEG_{5k}$ -29%-80 nm	$mPEG_{2k}$ -29%-80 nm	$mPEG_{5k}$ -29%-200 nm
Particle size (nm)	81.7 ± 0.9	82.5 ± 1.1	83.2 ± 1.8	86.2 ± 0.6	85.3 ± 0.9	211.5 ± 2.8
PDI	0.104 ± 0.010	0.113 ± 0.008	0.115 ± 0.010	0.108 ± 0.008	0.112 ± 0.008	0.102 ± 0.005
Zeta-potential (mV)	−1.22 ± 0.04	−1.25 ± 0.11	−1.27 ± 0.09	−1.33 ± 0.10	−1.24 ± 0.04	−1.28 ± 0.07
Entrapment efficiency (%)	22.43 ± 0.82	20.74 ± 0.5	21.49 ± 1.59	22.97 ± 1.39	21.69 ± 1.55	36.47 ± 1.56
Drug loading (%)	0.87 ± 0.03	0.79 ± 0.01	0.73 ± 0.03	0.62 ± 0.03	0.62 ± 0.02	0.62 ± 0.02
Fluorescence intensity ($\times 10^9$)	5.31 ± 0.15	5.17 ± 0.09	5.58 ± 0.22	5.10 ± 0.18	5.29 ± 0.13	5.31 ± 0.18

[a]Data are presented as mean ± SD ($n = 3$).

the initial fluorescence is maintained for at least 96 h in all formulations in purified water and PBS (Fig. 2B and C), indicating high fluorescence stability and simultaneously excluding potential leakage of the fluorophores and infiltration of water into PCL matrices—factors that could probably trigger untimely fluorescence quenching and thereby bring about interference[20]. In rat plasma, high fluorescence stability is also recorded for 72 h, but there is a slight declination in fluorescence as compared to observations in water and PBS (Fig. 2D), suggesting probable degradation of a small fraction of mPEG-PCL nanoparticles by enzymes in the plasma[48,49]. Fortunately, only about 10%−20% decrease in the initial fluorescence for at least 96 h ensures sufficient fluorescence recovery in plasma (Fig. 2D). Also, we monitored the particle size and PDI of mPEG-PCL nanoparticle following incubation with purified water and PBS except for rat plasma because of potential interference of plasma components (lipoproteins, albumins, etc.) with size measurement. The particle size and PDI are well maintained for all formulations in 96 h, indicating high stability of mPEG-PCL nanoparticles in these media (Supporting Information Fig. S1).

The possible leakage of DOX from mPEG-PCL nanoparticles was monitored following an *in vitro* release protocol. DOX-loaded mPEG-PCL nanoparticles were placed in dialysis bags and incubated in PBS in a shaker thermostatically maintained at 37 °C, and samples were detected for DOX by a fluorescence spectrophotometer. A slight burst release of approximately 16% of DOX from mPEG-PCL nanoparticles is observed after incubation for 4 h, and a maximal leakage of approximately 24% is observed for

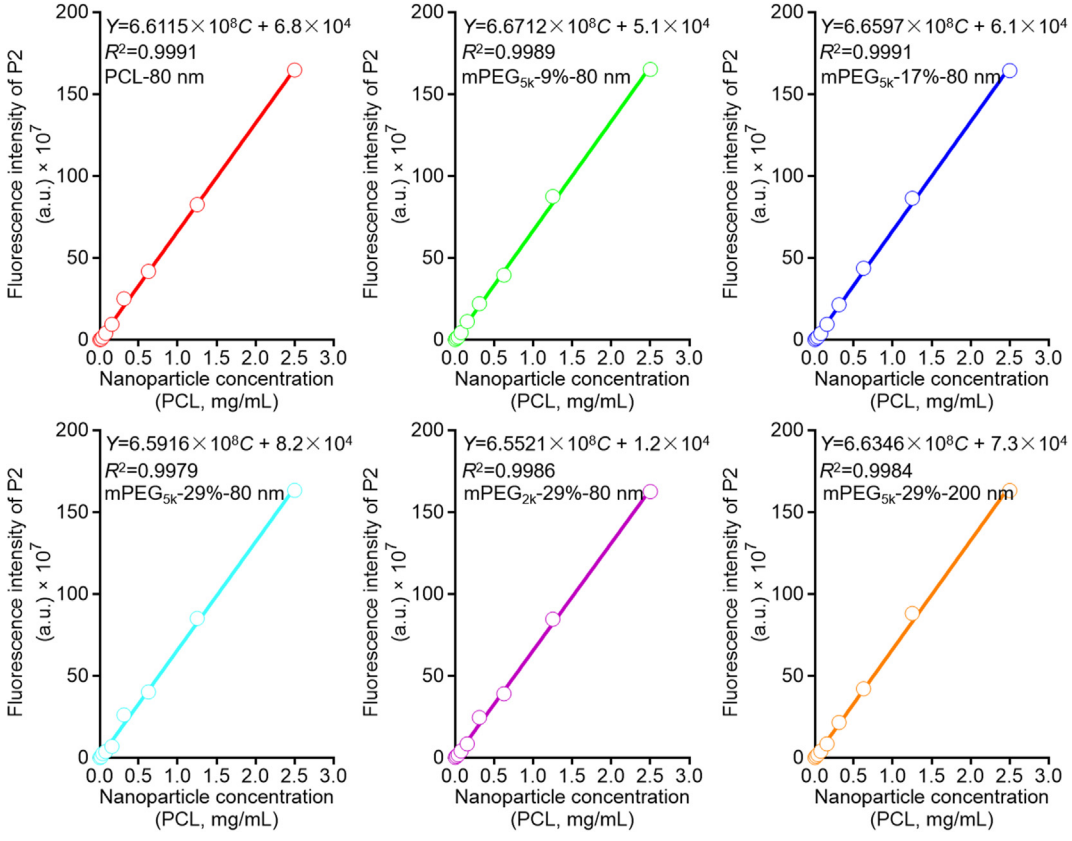

Figure 3 Calibration curves of mPEG-PCL nanoparticles in the blood obtained by linear regression of fluorescence intensity *vs.* nanoparticle concentration.

48 h (Fig. 2E). Increasing the particle size to 200 nm slows down the release rate with only 14% release of DOX from mPEG-PCL nanoparticles at 48 h as compared to 24% of the 80 nm group (Fig. 2E).

To quantify the content of mPEG-PCL nanoparticles in blood, an *in vitro* quantitative method was developed through establishing linearity between the concentration of nanoparticles and fluorescence intensity. Very good linearity is observed between fluorescent intensity (Y) and nanoparticle concentration (C, mg/mL) in the range of 0.0098−10 mg/mL for all formulations (Fig. 3). The precision and accuracy are determined at nanoparticle concentrations of 0.0048, 0.078, and 2.5 mg/mL, respectively. The intra- and inter-day precisions for all formulations are all below 10% (Supporting Information Tables S1–S2), while the accuracies fall within the range of 90%−110% for all formulations (Supporting Information Table S3). The validation data are in accordance with requirement of analysis of biological samples.

The kinetic profiles of mPEG-PCL nanoparticles in the blood as shown in Fig. 4 is typical of fast elimination from blood with typical "L"-type biphasic kinetics for all groups. In the non-decorated PCL-80 nm group, a large fraction of nanoparticles is cleaned from the blood rapidly with 65.7% *vs.* 5.1% of the initial dose left at 5 min and 2 h, respectively, after intravenous administration (Fig. 4A and D). It is no doubt that without PEG decoration, plain nanoparticles are easily opsonized by opsonins in the blood and then identified and captured by the MPS, resulting in a short half-life time in the blood[48]. To extend the circulation time in the blood, hydrophilic polymers, such as PEG, are coated on the surfaces of nanoparticles to form a hydration layer to circumscribe the attachment of opsonins[47,54]. PEG density and chain length are two important factors substantially influencing the circulation time of nanoparticles in the blood[55,56]. Though widely studied, past investigations generate deviated, even conflicting, results by monitoring of the payloads, drugs or emissive labels[48]. In this study, various factors are reassessed by monitoring of the particles quantitatively. It is found that even at a high density of PEG decoration, blood circulation time is not as long as commonly perceived. Even for the group with the longest expective circulation time, that is, the group with longer PEG chain length, higher coating density, and smaller particles size ($mPEG_{5k}$-29%-80 nm), approximately 25% of the nanoparticles are cleaned from the blood within 5 min; at 1 h, approximately 80% of the particles are cleaned (Fig. 4A and D). Nevertheless, increase in PEG density is obviously associated with a longer circulation time in the blood. Approximately 34.4% and 5.1% of the initially administered dose of non-PEGylated PCL nanoparticles (PCL-80 nm) are left in the blood at 15 min and 2 h, respectively, whereas the figures increase to 59.3% and 16.1% for the $mPEG_{5k}$-29%-80 nm group at corresponding time points, respectively. If taking AUC values as a measure for blood circulation, a positive correlation between the nanoparticle circulation and PEG coating density is established in the following order: mPEG-29% > mPEG-17% ≈ mPEG-9% > mPEG-0%, with AUC_{0-t} values 1.5, 1.2, and 1.3 times that of non-PEGylated nanoparticles (Fig. 5G). mPEG-PCL nanoparticles with shorter PEG chain lengths are cleaned more quickly from the blood after administration. In the $mPEG_{2K}$-29%-80 nm group, only 60.0% and 6.9% of the initial dose are left in the blood at 5 min and 2 h, respectively, whereas there are still 75.6% and 16.1% left for the higher PEG chain length group ($mPEG_{5K}$-29%-80 nm); a 1.4-time

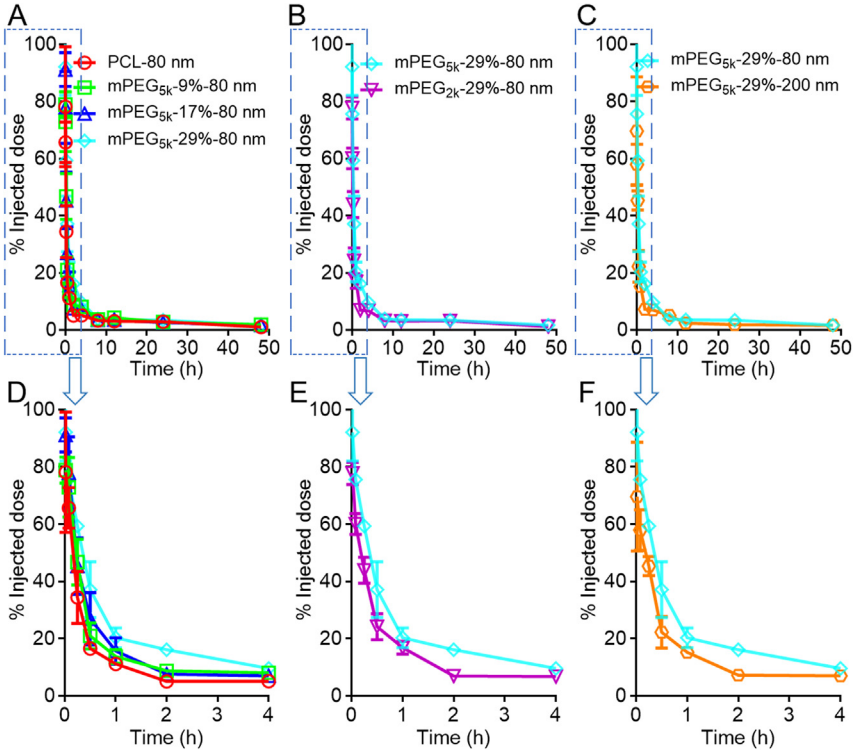

Figure 4 Blood kinetic profiles of mPEG-PCL nanoparticles in rats as highlighted by comparing PEGylation density (A), PEG chain length (B) and particle size (C), respectively. Plot D, E & F are enlargement of the 0−4 h regions of plot A, B and C, respectively. Data are presented as mean ± SD (n = 3).

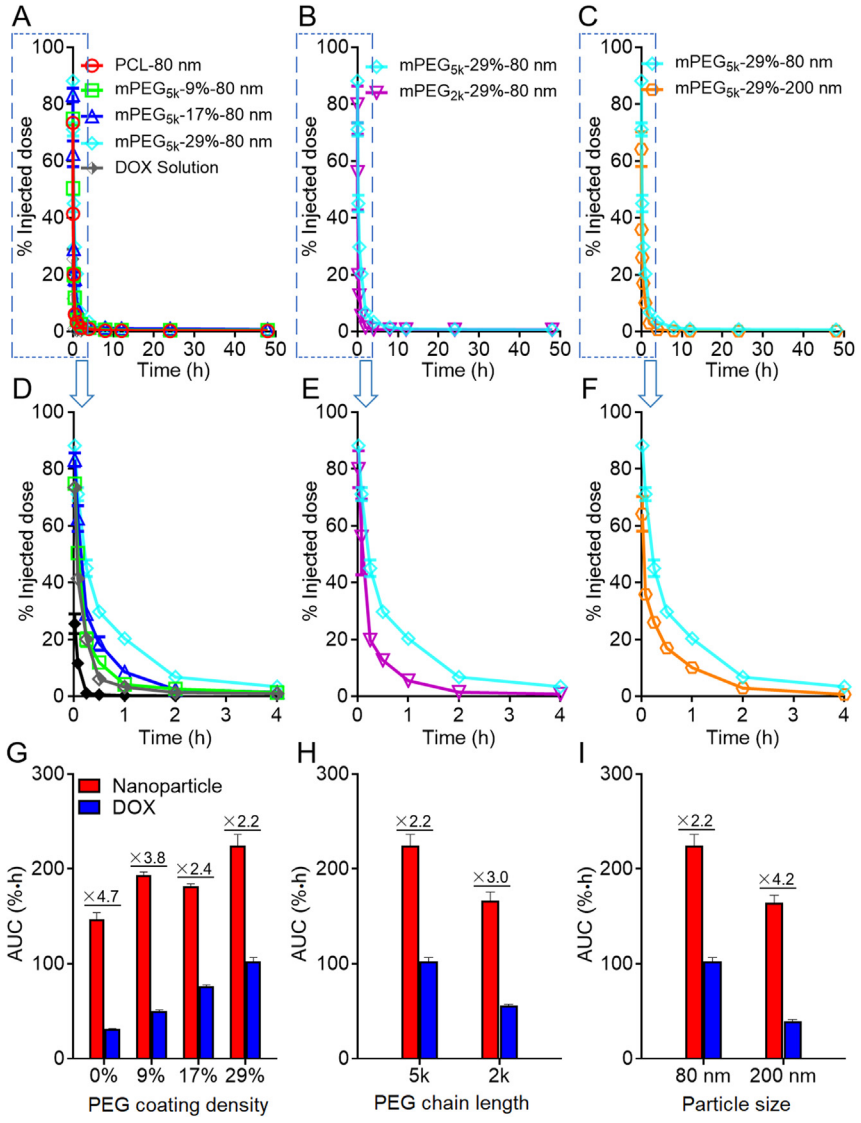

Figure 5 Blood pharmacokinetic profiles of DOX-loaded mPEG-PCL nanoparticle in rats as highlighted by comparing PEGylation density (A), PEG chain length (B) and particle size (C), respectively. Plot D, E & F are enlargement of the 0−4 h regions of plot A, B and C, respectively, while bar plot G, H & I present corresponding AUC values as summarized in Tables 2 and 3. Data are presented as mean ± SD (n = 3).

increase in the AUC value is observed in the mPEG$_{5k}$-29%-80 nm group (5k *vs.* 2k) (Figs. 4B, E, and 5H). Moreover, the blood kinetic process of mPEG-PCL nanoparticles with particle sizes of 80 and 200 nm is compared. Approximately 42% of the initially administered dose is cleaned from the blood at 15 min after administration, and only about 7.2% is left in the blood at 2 h in the 200 nm group. A reduction in particle size from 200 to 80 nm significantly prolongs the overall circulation time with a 1.4-time increase in AUC (Figs. 4C, F, and 5I).

Table 2 summarizes the kinetic parameters obtained by fitting to a two-compartmental model. In line with the rapid declination of the kinetic profiles of mPEG-PCL nanoparticles at early stages following administration, the $t_{1/2\alpha}$, elimination half time from the central compartment (CC), is very short, which however increases with higher PEG density, longer PEG chain length and decrease of particle size. On the contrary, the relatively longer $t_{1/2\beta}$ values bespeak slower elimination rate from the peripheral compartments (PC). The highest $t_{1/2\beta}$ values were obtained in the PCL-80 nm and PEG$_{5K}$-29%-200 nm groups, in line with a short half-life time in the blood than other PEGylated groups, indicating extended retention of nanoparticles without any PEG decoration or with bigger sizes in the PC. However, there is no regular rule observed in K_{10}, K_{12} and K_{21} values, which represent elimination constants from the CC, transport constant from CC to PC and transport constant from PC to CC, respectively, between the groups with different PEG chain length, coating density and particle size. The observation of similar mean residence time (MRT), another parameter utilized to represent the overall residence of nanoparticles in the body, in all groups indicates a similar retention time of mPEG-PCL nanoparticles *in vivo*.

Live imaging of mPEG-PCL nanoparticles in mice was carried out by utilizing IVIS (Fig. 6 and Supporting Information Fig. S7). At early stages after administration, the whole body exhibits strong fluorescence due to the perfusion of blood-borne

Table 2 Pharmacokinetic parameters of mPEG-PCL nanoparticle after intravenous injection of a single dose of mPEG-PCL nanoparticles in rats obtained by fitting to a two-compartmental model[a].

Parameter	PCL-80 nm	$mPEG_{5k}$-9%-80 nm	$mPEG_{5k}$-17%-80 nm	$mPEG_{5k}$-29%-80 nm	$mPEG_{2k}$-29%-80 nm	$mPEG_{5k}$-29%-200 nm
$t_{1/2\alpha}$ (h)	0.19 ± 0.10	0.24 ± 0.06	0.20 ± 0.10	0.3 ± 0.14	0.22 ± 0.04	0.27 ± 0.08
$t_{1/2\beta}$ (h)	15.29 ± 11.19	14.66 ± 2.44	12.58 ± 10.21	5.48 ± 1.21	5.4 ± 1.73	9.72 ± 3.79
K_{10} (L/h)	0.69 ± 0.44	0.38 ± 0.02	0.66 ± 0.41	0.55 ± 0.1	0.65 ± 0.09	0.45 ± 0.18
K_{12} (L/h)	3.44 ± 1.95	2.37 ± 0.71	2.83 ± 1.09	1.62 ± 0.66	2.06 ± 0.34	1.88 ± 0.43
K_{21} (L/h)	0.51 ± 0.47	0.34 ± 0.07	0.83 ± 0.99	0.58 ± 0.22	0.62 ± 0.19	0.41 ± 0.11
AUC_{0-t} (%·h)	147.02 ± 6.76	193.55 ± 3.28	181.93 ± 2.29	224.63 ± 11.76	166.28 ± 9.56	164.29 ± 8.07
MRT (h)	14.09 ± 0.53	14.55 ± 0.58	14.08 ± 0.52	12.95 ± 0.04	13.15 ± 0.35	14.03 ± 0.36

[a]Data are presented as mean ± SD ($n = 3$).

fluorescent mPEG-PCL nanoparticles. However, the fluorescence density declines rapidly in peripheral tissues and accumulated in the middle abdominal region where the liver, a major organ of the MPS, located beneath. As compared to the $mPEG_{5k}$-29%-80 nm group, a higher level of fluorescence is observed in the middle abdominal region for the PCL-80 nm and $mPEG_{5k}$-29%-200 nm groups as soon as 0.25 h after administration, which indicates that nanoparticles without PEG decoration or with a bigger size could be easily trapped by MPS and result in quick clearance from the blood. In addition, growing fluorescence is observed in peripheral tissues such as the limbs, snouts, and genitals, echoing findings in our previous studies[45,48,49]. By quantification of the regions of interest (ROI) in the live images, the distribution profiles of mPEG-PCL nanoparticles are depicted (Fig. 6B–K). Biphasic "L"-type distribution patterns are found in all groups, which are in parallel with the kinetic profiles in the blood. Phase I is characteristic of a fast-declining process, while phase II is an extended period with much lower fluorescence levels.

Fig. 7 and Supporting Information Fig. S8 show the images of mPEG-PCL nanoparticle distribution in main organs and tissues after administration. At 5 min, a low level of fluorescence is distributed widely in tissues of all groups, probably owing to blood perfusion. However, concentrated fluorescence is observed in the liver and spleen at 0.5 h and lasts up to 48 h. Very weak fluorescence is associated with the brain, implying the difficulty in crossing the blood–brain barrier (BBB). In addition, low levels of fluorescence present in the heart, lungs, kidneys, adrenal glands, vertebra, skin, and stomach, indicating limited distribution of nanoparticles in these tissues. For the comparison within the 80 nm groups, the results look predictable and consistent with normal knowledge that PEGylation reduces phagocytic uptake by organs in the MPS, including the liver, while enhancing long circulation in the blood. It is seemingly paradoxical that the mPEG5k-29%-200 nm group displays stronger fluorescence than the control group (PCL-80 nm). However, it should be marked that phagocytic uptake by the MPS is affected by a variety of factors with particle size being one of the leading factors. Obviously, in this case particle size overwhelms other factors in determining phagocytic uptake of nanocarriers. If compared under the same size, as done with the 80 nm groups, the effect of PEGylation could be clearly highlighted. Then, the content of nanoparticles in heart, liver, spleen, lungs, and kidneys is quantified. A calibration curve is established through linear regression between the concentration of mPEG-PCL nanoparticles and P2 fluorescence as measured by IVIS. There is a good linearity between total fluorescent intensity (Y) and nanoparticle concentration (C, mg/mL) in the range of 0.0048−2.5 mg/mL for all groups (Supporting Information Figs. S2–S6). Both intra- and inter-day precisions for all formulations are below 10% (Tables S1 and S2), while the accuracies are between 90 and 110% (Table S3), which is in accordance with the requirement for analysis of biological samples. In order to compare the kinetic profiles in a fixed scale, the data of each time points are normalized as percentages of the total dosage. Based on the quantification results, the kinetic profiles of mPEG-PCL nanoparticles in organs and tissues are depicted (Fig. 8 and Supporting Information Figs. S9–S12). As observed from the hepatic profiles (Fig. 8A–C), a high level of mPEG-PCL nanoparticles is distributed quickly in the liver, corresponding to the quick clearance of nanoparticles from the blood (Fig. 4), and it peaks quickly at 2−4 h for all groups. The rapid and high levels of hepatic accumulation of nanoparticles correspond to the "L"-type kinetic profiles in the blood. The deluge of nanoparticles from the circulation results in accumulation of nanoparticles in MPS organs such as the liver. In the non-decorated PCL-80 nm group, nanoparticles accumulate in the liver quickly and reach 82.5% of the administration dose at 2 h (Fig. 8A). In contrast to non-decorated nanoparticles, PEG decoration significantly reduces hepatic accumulation, especially in the PEG_{5k}-29%-80 nm group with the highest PEG coating density. At the highest, PEG decoration is able to reduce hepatic accumulation to a half of the level of the PCL-80 nm group (Fig. 8A). The AUC, a parameter utilized to represent blood exposure[48], of nanoparticle concentration *vs.* time profile in the liver shows a highly positive correlation between distribution content and PEG coating density in the order of mPEG-0% > mPEG-9% > mPEG-17% ≈ mPEG-29%, with AUC_{0-t} values approximately 2.2, 1.1, and 1.0 times that of the PEG_{5k}-29%-80 nm group (Fig. 8G). The PEG chain length has a positive effect on hepatic distribution of mPEG-PCL nanoparticles. PEG_{2k} decoration has an AUC 1.5 times that of $mPEG_{5k}$ decoration (Fig. 8B and H). Hepatic accumulation of nanoparticles is size-dependent because larger particles are prone to stimulate stronger phagocytosis by Kupffer cells, an important part of the MPS that always keep alert to take up nanoparticles. At the same PEG coating level, hepatic accumulation of 200 nm particles reaches 74.5% of the administration dose at 2 h *vs.* 40% for the 80 nm group (Fig. 8C). The smaller particles (80 nm) have prolonged circulation time together with less hepatic accumulation and a hepatic AUC 1.8 times less than that of the 200 nm particles (Fig. 8I). Spleen has the second highest distribution with 3%−6% of the administration dose accumulated (Supporting Information Fig. S10A–S10C). PEG decoration affects splenic accumulation as increase in PEG coating density and chain length is observed to decrease particle accumulation. Here, a high level of nanoparticles accumulates in the spleen in the 200 nm group, with an AUC_{0-t}

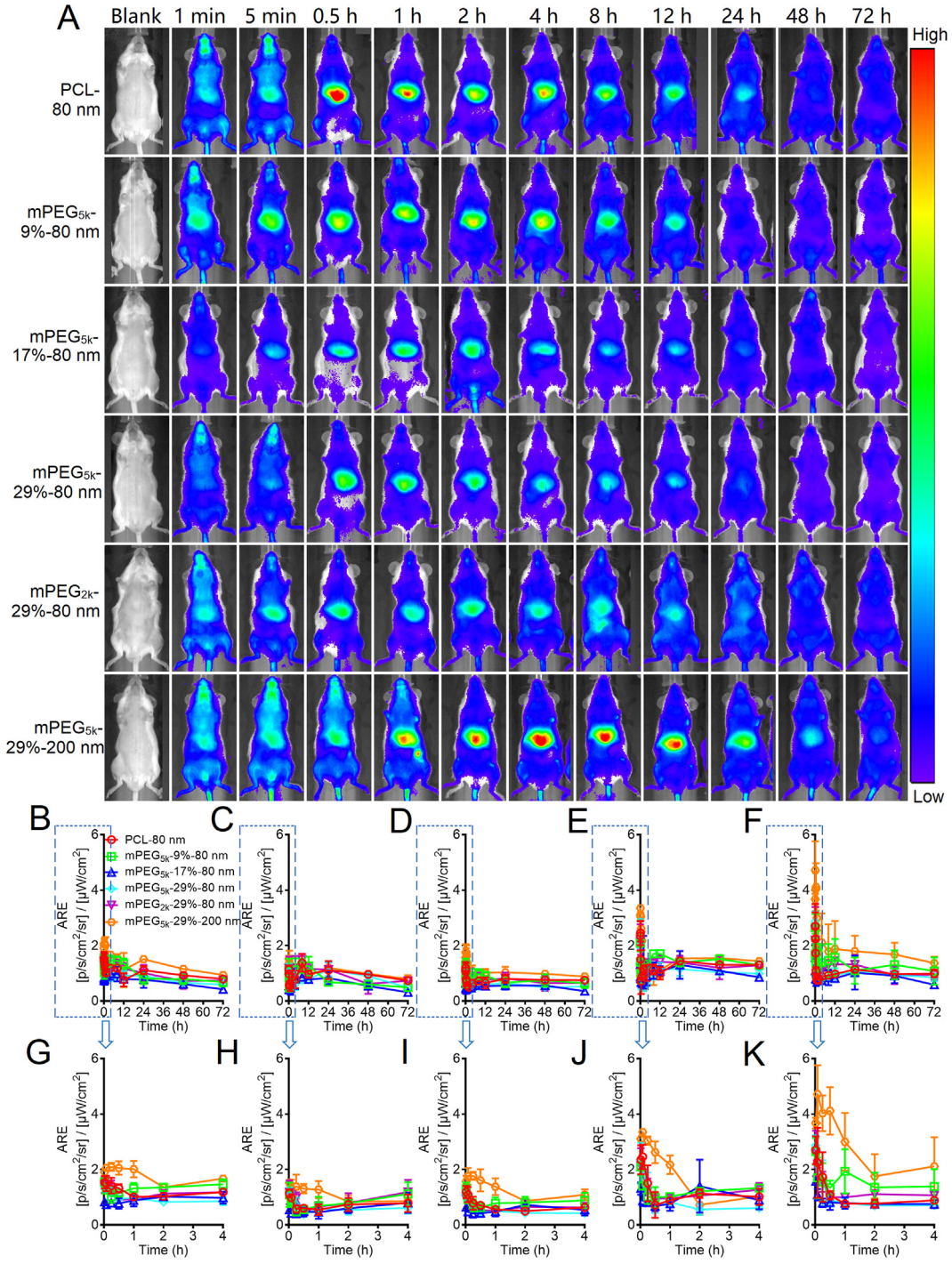

Figure 6 Live imaging of mPEG-PCL nanoparticle after intravenous administration to rats (A) and fractionized semi-quantification of fluorescence of regions of interest, which is presented as average radiant efficiency (ARE) that stands for the concentration of the nanoparticles: whole body (B), abdomen (C), limbs (D), genitals (E), snouts (F); and corresponding plots of enlargement (0−4 h) G, H, I, J, and K, respectively. Three animals are used for each group but only images of one animal are shown here. Please refer to Supporting Information Fig. S7 for a whole set of images. Data are presented as mean ± SD (n = 3).

value 1.6 times higher than that of the mPEG$_{5k}$-29%-80 nm group, which accelerates the clearance of nanoparticles from the blood (Fig. S10I). Less than 3% of the administered dose is distributed in the heart and lungs which however decreases after PEG decoration or reducing particle size, suggesting lower toxicity potentially associated with these organs (Figs. S9 and S11). As well, distribution of a low (<3%) level of mPEG-PCL nanoparticles in the kidneys indicates that nanoparticles are difficult to be filtered by the glomerulus and cleaned from blood in the kidneys (Supporting Information Fig. S12).

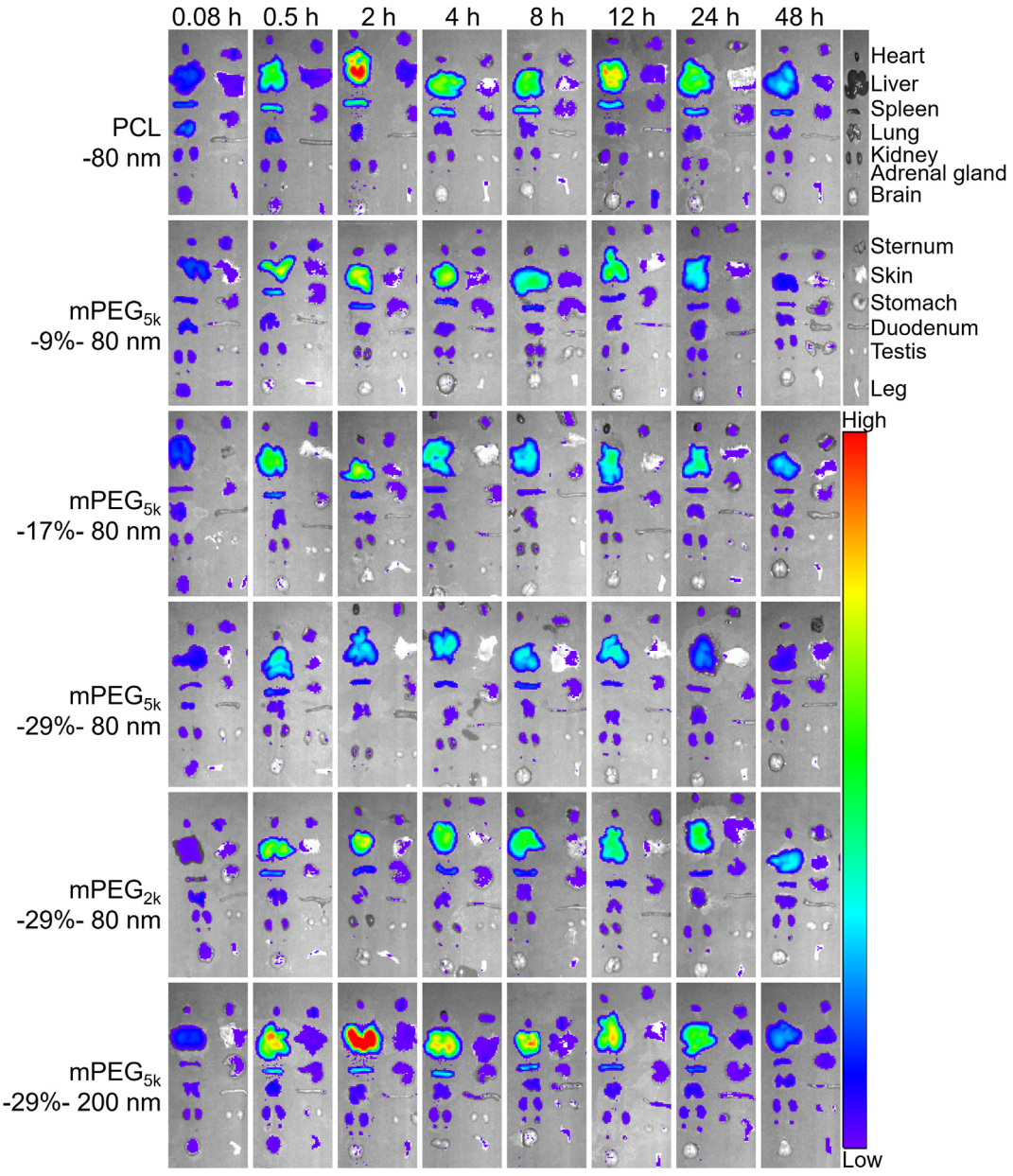

Figure 7 *Ex vivo* live imaging of dissected organs and tissues from mice after intravenous injection of P2-labeled mPEG-PCL nanoparticles. Only images of one animal are displayed for each time point. Please refer to Supporting Information Fig. S8 for a whole set of images.

The DOX content in the blood and tissues was measured by an HPLC method with a fluorescent detector[53]. DOX and the internal standard daunorubicin are well separated from the components extracted from blank blood and tissue homogenates. Good linearity is established between the peak area and concentration in the range of 0.039−10 μg/mL for both blood and tissue homogenates. The intra- and inter-day precisions are all below 10%, while the accuracies fall within the range of 90%−110% for all formulations. The validation data are in accordance with analytical requirement of biological samples.

The pharmacokinetics profiles of DOX are showed in Fig. 5A–F. The overall elimination rate from the blood is very fast with typical "L"-type biphasic kinetics for all formulations. About 30.0% *vs.* 90.0% of the initial dose is cleaned from the blood at 5 min and 2 h, respectively, after intravenous administration for all formulations. Approximately 20.0% and 3.2% of the initially administered DOX in non-PEGylated PCL nanoparticles (PCL-80 nm) are left in the blood at 15 min and 1 h, respectively, whereas the contents are 45.1% and 20.3% for the $mPEG_{5k}$-29%-80 nm group at the corresponding time points, respectively. In addition, a positive correlation between DOX circulation time and PEG coating density is established in the following order: mPEG-29% > mPEG-17% > mPEG-9% > mPEG-0%, with AUC_{0-t} values 3.3, 2.4, and 1.6 times that of non-PEGylated nanoparticles (Fig. 5G). DOX in mPEG-PCL nanoparticles with shorter PEG chain lengths are cleared more quickly from the blood after administration. In the $mPEG_{2K}$-29%-80 nm group, only 56.0% and 5.4% of the initial dose are left in blood at 5 min and 1 h, respectively, whereas there are still 71.1% and 20.3% left for the higher PEG chain length group ($mPEG_{5k}$-29%-80 nm). An 1.8-

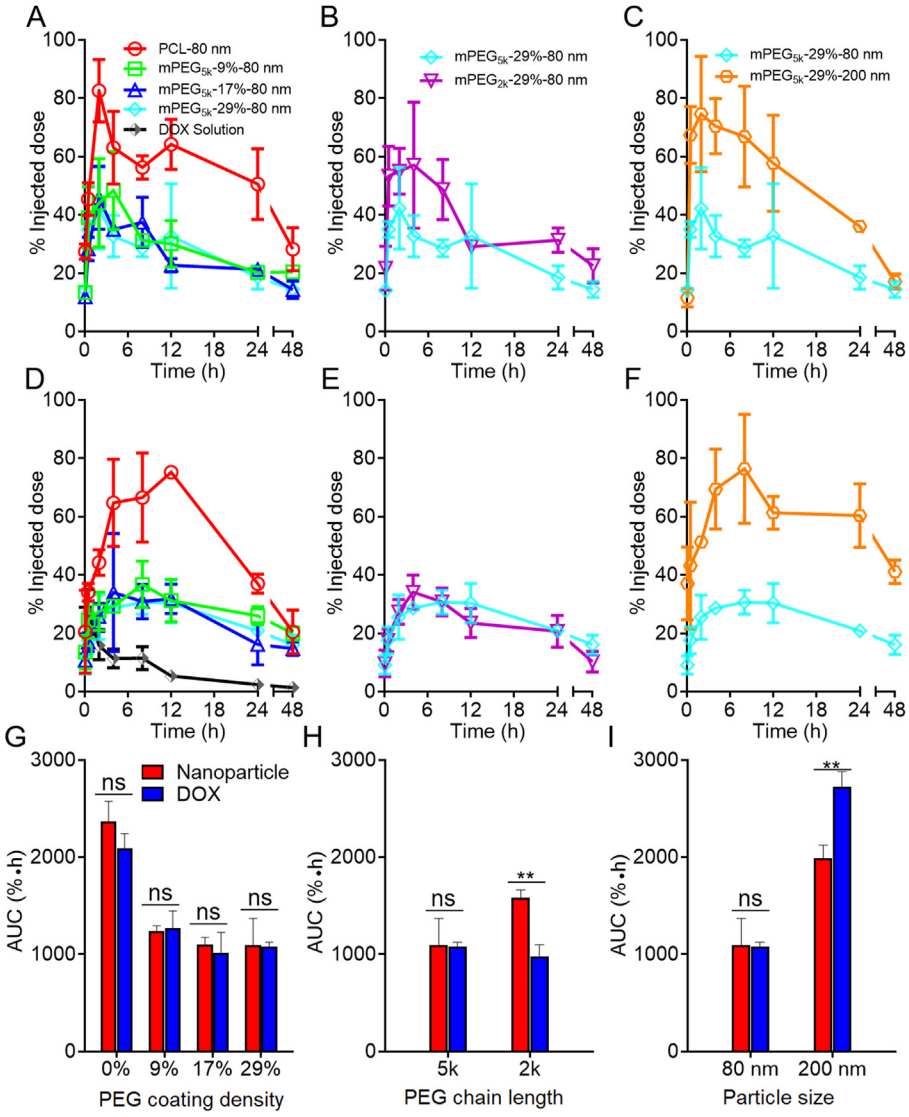

Figure 8 The profiles of the content of nanoparticles (A–C) and DOX (D–E) *vs.* time in the liver after intravenous administration of DOX-loaded mPEG-PCL nanoparticles as highlighted by comparing PEGylation density (A, D), PEG chain length (B, E), and particle size (C, F), respectively, while bar plot G, H & I present corresponding AUC values. Data are presented as mean ± SD ($n = 3$). $^{**}P < 0.01$. ns, not significant.

time increase in AUC is observed in the $mPEG_{5k}$-29%-80 nm group (5k *vs.* 2k) (Fig. 5B, E, and H). Moreover, DOX in mPEG-PCL nanoparticles with a bigger size are cleaned faster from the blood after administration. Approximately 35.8% of the initially administered dose is cleared from the blood 1 min after administration, and only about 17.0% is left in the blood at 0.5 h in the 200 nm group. A reduction in particle size from 200 to 80 nm significantly prolongs the overall circulation time of DOX with a 2.6-time increase in AUC (Fig. 5C, F, and I).

Table 3 summarizes the pharmacokinetic parameters obtained by fitting to a two-compartmental model. The $t_{1/2\alpha}$ is very low in all groups which is in accordance with the rapid declination of the pharmacokinetic profiles at the early stage after administration. However, a positive correlation between PEG decoration, particle size and $t_{1/2\alpha}$ is observed. Increasing the PEG coating density, chain length or decreasing the particle size helps increase the values of $t_{1/2\alpha}$. $T_{1/2\beta}$ is also very low in all groups, and its value increases as a result of PEG decoration. Both K_{10} and K_{12} correlate negatively with the blood circulation time of DOX, which however is subject to PEG coating density, chain length and particle size.

The DOX content in tissues as shown in Fig. 8D–F and Figs. S9–S12 is presented as percentages of the initially administered dose. A high level of DOX is distributed quickly in the liver for all groups after intravenous administration (Fig. 8D–F), corresponding to the quick clearance of DOX from the blood (Fig. 5). In the non-decorated PCL-80 nm group, DOX accumulates in the liver quickly and reached 75.2% of the administration dose at 12 h (Fig. 8D). In contrast to non-decorated nanoparticles, PEG decoration significantly reduces hepatic accumulation, especially in the PEG_{5k}-29%-80 nm group which had the highest PEG coating density (Fig. 8D). The AUC of DOX concentration *vs.* time profile in the liver shows a highly positive correlation between

Table 3 Pharmacokinetic parameters of DOX after intravenous injection of a single dose of DOX-loaded mPEG-PCL nanoparticles by fitting to a two-compartmental model in rats[a].

Parameter	PCL-80 nm	$mPEG_{5k}$-9%-80 nm	$mPEG_{5k}$-17%-80 nm	$mPEG_{5k}$-29%-80 nm	$mPEG_{2k}$-29%-80 nm	$mPEG_{5k}$-29%-200 nm	DOX
$t_{1/2\alpha}$ (h)	0.02 ± 0.01	0.09 ± 0.02	0.09 ± 0.03	0.11 ± 0.02	0.09 ± 0.04	0.02 ± 0.00	0.05 ± 0.01
$t_{1/2\beta}$ (h)	0.17 ± 0.01	0.73 ± 0.22	0.69 ± 0.31	0.9 ± 0.08	1.12 ± 1.02	0.53 ± 0.05	46.47 ± 39.56
K_{10} (L/h)	8.76 ± 5.79	3.03 ± 0.26	2.42 ± 0.13	1.38 ± 0.06	3.12 ± 0.51	2.63 ± 0.34	7.50 ± 0.70
K_{12} (L/h)	40.88 ± 49.48	3.96 ± 1.06	3.48 ± 1.07	2.53 ± 0.54	4.78 ± 2.76	15.96 ± 3.54	5.56 ± 2.26
K_{21} (L/h)	25.24 ± 7.80	2.42 ± 1.06	3.53 ± 2.22	3.25 ± 0.94	2.8 ± 2.23	13.45 ± 1.43	0.46 ± 0.70
AUC_{0-t} (%*h)	31.4 ± 0.45	50.34 ± 1.15	76.27 ± 1.48	102.43 ± 4.13	55.78 ± 1.47	39.14 ± 2.13	3.71 ± 0.21
MRT (h)	8.02 ± 0.24	11.57 ± 0.12	12.66 ± 0.41	8.72 ± 0.14	13.76 ± 0.28	4.78 ± 0.10	0.45 ± 0.00

[a]Data are presented as mean ± SD ($n = 3$).

distribution content and PEG density in the order of mPEG-0% > mPEG-9% > mPEG-17% ≈ mPEG-29%, with AUC_{0-t} values approximately 1.9, 1.2, and 0.9 times that of the PEG_{5k}-29%-80 nm group (Fig. 8G). The particle size has a positive effect on hepatic distribution of DOX. In contrast to 80 nm particle group, higher dose of DOX is distributed quickly in the liver in 200 nm group, with AUC_{0-t} values 2.5 times higher than the former (Fig. 8I). Spleen has the second highest distribution with accumulation of 3%−12% of the administration dose (Fig. S10D–S10F). PEG decoration has a positive correlation between distribution content and PEG density in the order of mPEG-0% > mPEG-9% > mPEG-17% > mPEG-29%, with AUC_{0-t} values 2.5, 1.8, and 1.1 times that of the $mPEG_{5k}$-29%-80 nm group (Fig. S11D and S11G). In addition, particle size has a critical effect on DOX accumulation in the spleen with less than 4% of splenic accumulation for the 80 nm group, whereas the content increases to 12% at 4 h after intravenous administration for the 200 nm group, with AUC_{0-t} value 3.3 times of the former (Fig. S10F and S10I). Only about 3% is distributed in the heart and lungs, suggesting reduced toxicity after administration for all formulations (Supporting Information Figs. S9 and S11). In contrast to approximate 3% accumulation in kidneys for all particle groups, more than 11% of DOX distribution in the kidneys is recorded at 5 min after intravenous administration of DOX solution (Fig. S12D).

It is difficult to monitor the *in vivo* release process of drug from nanoparticle after administration, due to the lack of effective tool to separate the free and nanoparticle-loaded drug from the complex *in vivo* environment. In this study, we analyze the *in vivo* leakage profile of DOX from mPEG-PCL nanoparticles through comparation of pharmacokinetics and kinetics of DOX-loaded mPEG-PCL nanoparticle. Although it is still hard to draw an accurate profile of *in vivo* drug release, the observation that the DOX pharmacokinetic profile deviates from the kinetic profiles suggests possible leakage of DOX in the blood after intravenous administration. Juxtaposing the pharmacokinetic and kinetic profiles of each formulation highlights the deviation of the two profiles in the blood. And the elimination rate of DOX in the blood is faster than nanoparticles for all groups. For example, in the PCL-80 nm group, approximately 41.4% and 0.3% of the initially administered dose of DOX are left in blood at 5 min and 12 h, respectively, whereas the figures are 65.6% and 3% for the particles at corresponding time points. The AUC_{0-t} value of particle content in the blood is at least 2.2 times higher than DOX in the blood for all formulations (Fig. 5G–I), indicating the DOX payloads are prematurely released from nanoparticles in the blood after intravenous administration. The effect of DOX leakage from nanoparticles in circulation on its subsequent distribution in organs is investigated. From Fig. 8, in contrast to DOX distribution, mPEG-PCL nanoparticles are accumulated in the liver faster for all formulations after intravenous administration. For example, approximate 82.5% of administration dose of particles is trapped in the liver at 2 h, whereas only 44.2% of the dose is accumulated at this time point for the PCL-80 nm group. From Fig. 8G–I, the AUC_{0-t} value of particle content in the liver is the same as DOX, indicating the liver as the biggest MPS organ is the main distribution location for particles and DOX though it is released prematurely in blood after intravenous administration. However, it should be concerned that due to the non-selective distribution of free DOX in hepatocytes whereas nanoparticle-encapsulated DOX is mainly captured by Kupffer cells, the leaked DOX may increase the damage of hepatocytes in the liver. Also, the accumulation of particles and DOX in other MPS organs is very low which is about 10% of the administration dose, indicating mPEG-PCL nanoparticles and DOX are safe to these organs. Using the targeting ability of nanoparticles, nanocarriers are taken to increase drug delivery to lesion sites, such as tumors, but in this study, we find that DOX is released prematurely from mPEG-PCL nanoparticles in the blood. Therefore, the impact of drug leakage on distribution of drug-loaded nanocarriers is yet to be investigated in the future.

4. Conclusions

Labeling the nanocarriers by a near-infrared fluorophore with absolute ACQ properties enables accurate bioimaging of mPEG-PCL nanoparticles. Moreover, quantification of integral nanocarriers is attempted, based on which the kinetic profiles of the nanocarriers are delineated. The profiles of the nanocarriers display fast clearance from the blood with typical "L"-type biphasic kinetics in spite of a high density of PEG decoration. More importantly, the pharmacokinetic profiles indicate faster clearance of DOX than the nanocarriers. The AUC_{0-t} values of the pharmacokinetic profiles are at least two times lower than those of the particle kinetic profiles. The nanocarriers obviously circulate longer than DOX in the blood, suggesting possible leakage of DOX from the nanocarriers after intravenous administration. Hepatic accumulation is the highest among the organs and tissues investigated for each group of different PEG coating levels, which however is reversely proportionate to the blood circulation time. The concentration of nanoparticles is higher than DOX concentration in early stage of hepatic accumulation as a result of instant but immature leakage of DOX from the nanocarriers in the circulation. The distribution of the nanoparticles in other tissues is

relatively low as compared with the liver and blood. It is concluded that pegylation and reduction in particle size lead to extended circulation of drug nanocarriers in the blood with simultaneous decrease in uptake by various organs of the MPS. The long-circulating effect of mPEG-PCL nanoparticles is reassured by monitoring of either DOX or the nanocarriers, but the faster clearance of DOX implies premature leakage of a fraction of the payloads after intravenous administration. The findings of this study suggest that both the long-circulating effect and the delivery capacity of drug nanocarriers should not be exaggerated under certain circumstances. The crucial information obtained may be of translational significance in guiding the designing of drug nanocarriers towards optimization of therapeutic efficacy while reducing toxic adverse effect.

Acknowledgments

This work was supported by the National Natural Science Foundation of China (Nos. 81872815, 82030107, and 81690263) and Science and Technology Commission of Shanghai Municipality (No. 19XD1400300, China). We are grateful to Prof. Chen Jiang at School of Pharmacy, Fudan University for her help with determination of doxorubicin.

Author contributions

Wei Wu provided supervision. Wei Wu, Yi Lu, and Jianping Qi designed the research. Wufa Fan carried out the experiments and performed data analysis. Haixia Peng, Luting Wang, Haisheng He, Yuhua Ma, and Zhou Yu participated part of the experiments. Wufa Fan wrote the manuscript. Wei Wu and Wufa Fan revised the manuscript. All of the authors have read and approved the final manuscript.

Conflicts of interest

The authors have no conflicts of interest to declare.

Appendix A. Supporting information

Supporting data to this article can be found online at https://doi.org/10.1016/j.apsb.2021.11.016.

References

1. Gadekar V, Borade Y, Kannaujia S, Rajpoot K, Anup N, Tambe V, et al. Nanomedicines accessible in the market for clinical interventions. *J Control Release* 2021;**330**:372–97.
2. Li J, Burgess DJ. Nanomedicine-based drug delivery towards tumor biological and immunological microenvironment. *Acta Pharm Sin B* 2020;**10**:2110–24.
3. Gonzalez-Valdivieso J, Girotti A, Schneider J, Arias FJ. Advanced nanomedicine and cancer: challenges and opportunities in clinical translation. *Int J Pharm* 2021;**599**:120438.
4. Germain M, Caputo F, Metcalfe S, Tosi G, Spring K, Åslund AKO, et al. Delivering the power of nanomedicine to patients today. *J Control Release* 2020;**326**:164–71.
5. Anselmo AC, Mitragotri S. Nanoparticles in the clinic. *Bioeng Transl Med* 2016;**1**:10–29.
6. Anselmo AC, Mitragotri S. Nanoparticles in the clinic: an update. *Bioeng Transl Med* 2019;**4**:10143.
7. Wu W, Li T. Unraveling the *in vivo* fate and cellular pharmacokinetics of drug nanocarriers. *Adv Drug Deliv Rev* 2019;**143**:1–2.
8. Wu W, Li T, Zheng Y. The biological fate of drug nanocarriers. *Acta Pharm Sin B* 2021;**11**:850–1.
9. Zhao Z, Ukidve A, Krishnan V, Mitragotri S. Effect of physicochemical and surface properties on *in vivo* fate of drug nanocarriers. *Adv Drug Deliv Rev* 2019;**143**:3–21.
10. Chaw SY, Novera W, Chacko AM, Wong TTL, Venkatraman S. *In vivo* fate of liposomes after subconjunctival ocular delivery. *J Control Release* 2021;**329**:162–74.
11. Wang W, Huang Z, Xue K, Li J, Wang W, Ma J, et al. Development of aggregation-caused quenching probe-loaded pressurized metered-dose inhalers with fluorescence tracking potentials. *AAPS PharmSciTech* 2020;**21**:296.
12. Huang Z, Huang Y, Wang W, Fu F, Wang W, Dang S, et al. Relationship between particle size and lung retention time of intact solid lipid nanoparticle suspensions after pulmonary delivery. *J Control Release* 2020;**325**:206–22.
13. Man F, Gawne PJ, de Rosales RTM. Nuclear imaging of liposomal drug delivery systems: a critical review of radiolabelling methods and applications in nanomedicine. *Adv Drug Deliv Rev* 2019;**143**:134–60.
14. Lu Y, Lv Y, Li T. Hybrid drug nanocrystals. *Adv Drug Deliv Rev* 2019;**143**:115–33.
15. Tang H, Rui M, Mai J, Guo W, Xu Y. Reimaging biological barriers affecting distribution and extravasation of PEG/peptide-modified liposomes in xenograft SMMC7721 tumor. *Acta Pharm Sin B* 2020;**10**:546–56.
16. Hu X, Dong X, Lu Y, Qi J, Zhao W, Wu W. Bioimaging of nanoparticles: the crucial role of discriminating nanoparticles from free probes. *Drug Discov Today* 2017;**22**:382–7.
17. Hollis CP, Weiss HL, Leggas M, Evers BM, Gemeinhart RA, Li T. Biodistribution and bioimaging studies of hybrid paclitaxel nanocrystals: lessons learned of the EPR effect and image-guided drug delivery. *J Control Release* 2013;**172**:12–21.
18. Liu Y, Tseng YC, Huang L. Biodistribution studies of nanoparticles using fluorescence imaging: a qualitative or quantitative method? *Pharm Res* 2012;**29**:3273–7.
19. Meng F, Wang J, Ping Q, Yeo Y. Quantitative assessment of nanoparticle biodistribution by fluorescence imaging, revisited. *ACS Nano* 2018;**12**:6458–68.
20. Qi J, Hu X, Dong X, Lu Y, Lu H, Zhao W, et al. Towards more accurate bioimaging of drug nanocarriers: turning aggregation-caused quenching into a useful tool. *Adv Drug Deliv Rev* 2019;**143**:206–25.
21. Chen T, He B, Tao J, He Y, Deng H, Wang X, et al. Application of Förster Resonance Energy Transfer (FRET) technique to elucidate intracellular and *in vivo* biofate of nanomedicines. *Adv Drug Deliv Rev* 2019;**143**:177–205.
22. Wang Y, Zhang Y, Wang J, Liang XJ. Aggregation-induced emission (AIE) fluorophores as imaging tools to trace the biological fate of nano-based drug delivery systems. *Adv Drug Deliv Rev* 2019;**143**:161–76.
23. Qi J, Lu Y, Zhao W, Dong X, Wu W. *In vivo* fate study of drug nanocarriers: the applications of environment-responsive fluorescent dyes. *Acta Pharm Sin* 2019;**54**:1965–75.
24. Zhang J, Corpstein Li T. Intracellular uptake of nanocrystals: probing with aggregation-induced emission of fluorescence and kinetic modeling. *Acta Pharm Sin B* 2021;**11**:1069–82.
25. Liu W, Li D, Dong Z, Liu K, He H, Lu Y, et al. Insight into the *in vivo* translocation of oral liposomes by fluorescence resonance energy transfer effect. *Int J Pharm* 2020;**587**:119682.
26. Sun X, Wang G, Zhang H, Hu S, Liu X, Tang J, et al. The blood clearance kinetics and pathway of polymeric micelles in cancer drug delivery. *ACS Nano* 2018;**12**:6179–92.
27. Gao W, Lee D, Meng Z, Li T. Exploring intracellular fate of drug nanocrystals with crystal-integrated and environment-sensitive fluorophores. *J Control Release* 2017;**267**:214–22.
28. Lin Z, Xi L, Chen S, Tao J, Wang Y, Chen X, et al. Uptake and trafficking of different sized PLGA nanoparticles by dendritic cells in

imiquimod-induced psoriasis-like mice model. *Acta Pharm Sin B* 2021;**11**:1047−55.
29. Andreiuk B, Reisch A, Bernhardt E, Klymchenko AS. Fighting aggregation-caused quenching and leakage of dyes in fluorescent polymer nanoparticles: universal role of counterion. *Chem Asian J* 2019;**14**:836−46.
30. Tsai WK, Wang CI, Liao CH, Yao CN, Kuo TJ, Liu MH, et al. Molecular design of near-infrared fluorescent Pdots for tumor targeting: aggregation-induced emission *versus* anti-aggregation-caused quenching. *Chem Sci* 2018;**10**:198−207.
31. Hu X, Zhang J, Yu Z, Xie Y, He H, Qi J, et al. Environment-responsive aza-BODIPY dyes quenching in water as potential probes to visualize the *in vivo* fate of lipid-based nanocarriers. *Nanomedicine* 2015;**11**:1939−48.
32. Wang W, Huang Z, Li Y, Wang W, Shi J, Fu F, et al. Impact of particle size and pH on protein corona formation of solid lipid nanoparticles: a proof-of-concept study. *Acta Pharm Sin B* 2021;**11**:1030−46.
33. Xia F, Chen Z, Zhu Q, Qi J, Dong X, Zhao W, et al. Gastrointestinal lipolysis and trans-epithelial transport of SMEDDS *via* oral route. *Acta Pharm Sin B* 2021;**11**:1010−20.
34. Wang X, Qiu L, Wang X, Ouyang H, Li T, Han L, et al. Evaluation of intestinal permeation enhancement with carboxymethyl chitosan-rhein polymeric micelles for oral delivery of paclitaxel. *Int J Pharm* 2020;**573**:118840.
35. Hu X, Fan W, Yu Z, Lu Y, Qi J, Zhang J, et al. Evidence does not support absorption of intact solid lipid nanoparticles *via* oral delivery. *Nanoscale* 2016;**8**:7024−35.
36. Ahmad E, Feng Y, Qi J, Fan W, Ma Y, He H, et al. Evidence of nose-to-brain delivery of nanoemulsions: cargoes but not vehicles. *Nanoscale* 2017;**9**:1174−83.
37. Xia F, Fan W, Jiang S, Ma Y, Lu Y, Qi J, et al. Size-dependent translocation of nanoemulsions *via* oral delivery. *ACS Appl Mater Interfaces* 2017;**9**:21660−72.
38. Yang Y, Lv Y, Shen C, Shi T, He H, Qi J, et al. *In vivo* dissolution of poorly water-soluble drugs: proof of concept based on fluorescence bioimaging. *Acta Pharm Sin B* 2021;**11**:1056−68.
39. Xie Y, Shi B, Xia F, Qi J, Dong X, Zhao W, et al. Epithelia transmembrane transport of orally administered ultrafine drug particles evidenced by environment sensitive fluorophores in cellular and animal studies. *J Control Release* 2018;**270**:65−75.
40. Yuan H, Zhao W, Wu W. How can aggregation-caused quenching based bioimaging of drug nanocarriers be improved? *Ther Deliv* 2020;**11**:809−12.
41. He H, Wang L, Ma Y, Yang Y, Lv Y, Zhang Z, et al. The biological fate of orally administered mPEG-PDLLA polymeric micelles. *J Control Release* 2020;**327**:725−36.
42. Shi T, Lv Y, Huang W, Fang Z, Qi J, Chen Z, et al. Enhanced transdermal delivery of curcumin nanosuspensions: a mechanistic study based on co-localization of particle and drug signals. *Int J Pharm* 2020;**588**:119737.
43. Zoya I, He H, Wang L, Qi J, Lu Y, Wu W. The intragastrointestinal fate of paclitaxel-loaded micelles: implications on oral delivery. *Chin Chem Lett* 2021;**32**:1545−9.
44. Fan W, Yu Z, Peng H, He H, Lu Y, Qi J, et al. Effect of particle size on the pharmacokinetics and biodistribution of parenteral nanoemulsions. *Int J Pharm* 2020;**586**:119551.
45. Yang J, Dong Z, Liu W, He H, Lu Y, Wu W, et al. Discriminating against injectable fat emulsions with similar formulation based on water quenching fluorescent probe. *Chin Chem Lett* 2020;**31**:875−9.
46. Shen B, Shen C, Zhu W, Yuan H. Integral nanocrystals absorption exhibits high contribution to oral bioavailability enhancement of quercetin. *Acta Pharm Sin B* 2021;**11**:978−88.
47. Wang R, Zhang Z, Liu B, Xue J, Liu F, Tang T, et al. Strategies for the design of nanoparticles: starting with long-circulating nanoparticles, from lab to clinic. *Biomater Sci* 2021;**9**:3621−37.
48. He H, Jiang S, Xie Y, Lu Y, Qi J, Dong X, et al. Reassessment of long circulation *via* monitoring of integral polymeric nanoparticles justifies a more accurate understanding. *Nanoscale Horiz* 2018;**3**:397−407.
49. He H, Zhang J, Xie Y, Lu Y, Qi J, Ahmad E, et al. Bioimaging of intravenous polymeric micelles based on discrimination of integral particles using an environment-responsive probe. *Mol Pharm* 2016;**13**:4013−9.
50. Zhao W, Carreira EM. Conformationally restricted aza-bodipy: a highly fluorescent, stable, near-infrared-absorbing dye. *Angew Chem Int Ed Engl* 2005;**44**:1677−9.
51. Zhao W, Carreira EM. Conformationally restricted aza-BODIPY: highly fluorescent, stable near-infrared absorbing dyes. *Chemistry* 2006;**12**:7254−63.
52. Lv Y, He H, Qi J, Lu Y, Zhao W, Dong X, et al. Visual validation of the measurement of entrapment efficiency of drug nanocarriers. *Int J Pharm* 2018;**547**:395−403.
53. Zhang Y, Guo Q, An S, Lu Y, Li J, He X, et al. ROS-switchable polymeric nanoplatform with stimuli-responsive release for active targeted drug delivery to breast cancer. *ACS Appl Mater Interfaces* 2017;**9**:12227−40.
54. Moghimi SM, Hunter AC, Murray JC. Long-circulating and target-specific nanoparticles: theory to practice. *Pharmacol Rev* 2001;**53**:283−318.
55. Mosqueira VC, Legrand P, Morgat JL, Vert M, Mysiakine E, Gref R, et al. Biodistribution of long-circulating PEG-grafted nanocapsules in mice: effects of PEG chain length and density. *Pharm Res* 2001;**18**:1411−9.
56. Ait Bachir Z, Huang Y, He M, Huang L, Hou X, Chen R, et al. Effects of PEG surface density and chain length on the pharmacokinetics and biodistribution of methotrexate-loaded chitosan nanoparticles. *Int J Nanomed* 2018;**13**:5657−71.